Acta Crystallographica Section D
Biological Crystallography
ISSN 0907-4449

Structure of native phosphoglucose isomerase from rabbit: conformational changes associated with catalytic function

Christopher Davies[a]* and Hilary Muirhead[b]

[a]Department of Biochemistry and Molecular Biology, Medical University of South Carolina, Charleston, SC 29425, USA, and [b]Department of Biochemistry, School of Medical Sciences, University of Bristol, Bristol BS8 1TD, England

Correspondence e-mail: davies@musc.edu

Received 5 September 2002
Accepted 19 December 2002

PDB Reference: rabbit PGI, 1n8t, r1n8tsf.

Phosphoglucose isomerase (PGI) is a housekeeping enzyme of metabolism that catalyses the interconversion of glucose 6-phosphate and fructose 6-phosphate, with roles in the glycolytic and gluconeogenic pathways. PGI is also a multifunctional protein that manifests the properties of a cytokine in a wide array of cellular processes, including the production of immunoglobulin by B cells and tumour-cell differentiation. The crystal structure of PGI in the native form from rabbit muscle has been solved at a resolution of 2.5 Å by a combination of multiple isomorphous replacement and multi-crystal averaging techniques. Comparison with published structures of rabbit PGI in complex with three inhibitors and with the substrate fructose 6-phosphate reveals a number of conformational changes that may be associated with catalytic function. These occur in the small domain around the sugar phosphate-binding site, in a small helix carrying His388 and in a helix near the C-terminal end. One of these may be the structural rearrangement that has been postulated to be the rate-limiting step for catalysis.

1. Introduction

Phosphoglucose isomerase (PGI; EC 5.3.1.9) [also known as glucose 6-phosphate isomerase (GPI) and phosphohexose isomerase (PHI)] is a key enzyme in glycolysis and gluconeogenesis that catalyses the interconversion of glucose 6-phosphate (G6P) and fructose 6-phosphate (F6P). This is an equilibrium reaction whose direction is determined solely by the relative proportions of F6P and G6P in the cytosol.

PGI is a member of the aldose–ketose isomerase class of enzymes. These catalyse the interconversion of aldose and ketose by transfer of a carbon-bound hydrogen between C1 and C2. Since PGI exchanges protons with solvent, it is believed that the mechanism proceeds through proton transfer *via* a *cis*-enediol intermediate (Rose, 1975). Given the scarcity of open-chain forms of G6P and F6P in solution (Swenson & Barker, 1971) and the high turnover of the enzyme, PGI is likely to also catalyse ring opening. Despite a flurry of high-resolution structures from *Bacillus stearothermophilus* (Sun *et al.*, 1999), rabbit (Jeffery *et al.*, 2000), human (Read *et al.*, 2001) and pig (Davies & Muirhead, 2002) sources, the catalytic mechanism of PGI remains debatable. Based on structural and biochemical evidence, two possibilities for the base catalyst have been proposed: a histidine (Jeffery *et al.*, 2000; Meng *et al.*, 1999) or a glutamate (Jeffery *et al.*, 2001; Read *et al.*, 2001). The identity of the amino acid responsible for ring opening is also questionable, with the best candidates being a lysine or histidine.

© 2003 International Union of Crystallography
Printed in Denmark – all rights reserved

Interest in PGI has grown significantly in recent years following the discovery that it is a multifunctional protein. Thus, inside the cell PGI is a housekeeping enzyme of sugar metabolism, but outside the cell PGI exhibits the properties of a cytokine. The first reports linked PGI with the previously characterized lymphokine neuroleukin (NLK; Chaput *et al.*, 1988; Faik *et al.*, 1988). NLK is a 56 kDa monomeric product of lectin-stimulated T cells that promotes the survival of spinal and sensory neurons in culture (Gurney, Apatoff *et al.*, 1986; Gurney, Heinrich *et al.*, 1986). In recent years, PGI has also been linked to several other factors: autocrine motility factor (AMF; Watanabe *et al.*, 1996), maturation factor (MF; Xu *et al.*, 1996), an antigen in rheumatoid arthritis (Matsumoto *et al.*, 1999) and sperm agglutination (Yakirevich & Naot, 2000) and, finally, a novel serine-protease inhibitor (MBSPI; Cao *et al.*, 2000). Where tested, the identity of PGI with these factors has been confirmed by PGI enzyme activity in NLK (Gurney, 1988), AMF (Watanabe *et al.*, 1996) and MF (Xu *et al.*, 1996). Conversely, commercially available PGI from rabbit muscle (the subject of this study) manifests MF (Xu *et al.*, 1996) and AMF properties (Watanabe *et al.*, 1996). How the cytokine properties of PGI are related to its enzymatic function remains unknown. The enzyme is of further medical interest because mutations in PGI are associated with haemolytic anaemia (Baughan *et al.*, 1968) and because high levels of serum PGI activity are linked with several human cancers (Baumann *et al.*, 1990).

Several crystal structures of the rabbit enzyme complexed with the active-site inhibitors 6-phosphogluconate, 5-phosphoarabinonate, 5-phosphoarabinonohydroxamic acid and with the substrate fructose 6-phosphate are available, but none to date are of the unbound enzyme. In the absence of the enzyme in its native form, a true picture of the structural changes induced by ligand binding is not clear. In this paper, we report the 2.5 Å structure of the native enzyme from rabbit muscle, solved by a combination of molecular replacement, heavy-atom derivatives and multi-crystal averaging. The structure is compared to the ligand-bound structures to reveal evidence of conformational changes that may be involved in catalysis.

2. Experimental

2.1. Crystallization

Rabbit PGI is commercially available as a crystalline suspension (Sigma). Using 1 ml of the suspension, the crystals were spun out of solution and redissolved in 2 ml of buffer containing 25 m*M* imidazole pH 8.2, 0.1% β-mercaptoethanol and 1 m*M* EDTA. The protein was then concentrated using Centricon-10 microconcentrators (Amicon) and diluted with a further 2 ml of buffer. After 2–3 concentrate/wash cycles the protein was concentrated to an absorbance of 6 at 280 nm, corresponding to about 5 mg ml^{-1}. Initial crystallization trials were by the standard hanging-drop method in which 3 µl of protein and 3 µl of well solution were mixed and equilibrated over 0.7 ml of well solution. Initial trials used Crystal Screens I and II (Hampton Research). Crystals of rabbit PGI were obtained over wells containing 12–14% PEG 6000 and Tris–HCl buffer pH 6.8–7.5. These belong to space group $C222_1$, with unit-cell parameters a = 83.1, b = 115.2 and c = 271.5 Å under cryoconditions, and diffract to at least 1.9 Å. The estimated solvent content indicates that there is one dimer in the asymmetric unit.

Table 1
Data-collection and phasing statistics.

Values in parentheses are for the highest resolution shell.

Data	Native	$PtCl_4$	$HgCl_2$
Molarity (m*M*)	—	1	0.25
Length of soak	—	3 d	5 h
Reflections (measured)	166547	45250	35803
Reflections (unique)	47443	18700	20835
Completeness (%)	91.6 (68.8)	88.4 (82.0)	70.5 (67.4)
Data with $I > 3\sigma(I)$ (%)	83.9 (70.2)	73.7 (52.9)	95.4 (96.2)
Resolution (Å)	2.4	3.4	2.9
R_{sym}†	5.5 (18.4)	7.4 (19.3)	4.4 (7.6)
R_{merge}‡	—	15.0	12.6
No. of sites	—	6	5
Resolution used for phasing (Å)	—	3.3	3.0
Phasing power§, centric/acentric	—	1.43/1.01	1.16/0.95
R_{Cullis}¶, centric/acentric	—	0.89/0.90	0.82/0.77

† $R_{sym} = \sum|I_I - I_M|/\sum I_M$, where I_I is the intensity of the measured reflection and I_M is the mean intensity of all symmetry-related reflections. ‡ $R_{merge} = \sum|F_{PH} - F_P|/\sum|F_{PH}|$. § Phasing power = $F_H/E_{r.m.s.}$. ¶ $R_{Cullis} = \sum(F_{PH} \pm F_P) - F_H(\text{calc})/\sum|F_{PH} - F_P|$. F_P, F_{PH} and F_H are the protein, derivative and heavy-atom structure factors, respectively, and $E_{r.m.s.}$ is the residual lack of closure.

2.2. Data collection

Native diffraction data were collected using an R-AXIS II imaging-plate system mounted on an RU-200 rotating-anode generator (Rigaku-MSC) operating at 40 kV and 80 mA and fitted with Yale mirror optics. The crystals were soaked in mother liquor (15% PEG 6000, 50 m*M* Tris–HCl pH 7.0) containing 30% glycerol as a cryoprotectant and then flash-frozen at 100 K. The crystal-to-detector distance was 190 mm, with a 2θ offset angle of 12°. Frames were collected in 2.5° oscillations with 30 min exposure time per frame. A total of 165° of data were collected. The data from one derivative ($PtCl_4$) were collected using the R-AXIS II system, with a crystal-to-detector distance of 220°, an offset angle of 5°, an oscillation angle of 3° and an exposure time of 35 min per frame. A total of 111° of data were collected. Data from a second derivative ($HgCl_2$) were collected using a DIP2030 area-detector system (MacScience) mounted on a Nonius FR591 X-ray generator operating at 45 kV and 90 mA and equipped with focusing mirrors (MacScience). The crystal-to-detector distance was 250 mm, with no offset angle, and frames were collected in 1° oscillations with an exposure time of 12 min. Because of a technical problem, it was only possible to collect 35° of data. All data were processed using *HKL* (Otwinowski & Minor, 1997).

2.3. Phasing

The program *AMoRe* (Navaza, 1994) was used to solve a preliminary structure of rabbit PGI using a partially refined structure of the pig enzyme as a search model. However, the resulting phases calculated from this model were poor and of insufficient quality to undertake any meaningful revision to the model (Fig. 1*a*). To obtain phases without model bias, a search for heavy-atom derivatives was undertaken. For this, crystals were soaked in solutions containing heavy atoms, passed through the cryoprotectant solution and flash-frozen. After data collection, difference Fourier maps were used to identify the heavy-atom sites in each derivative calculated using *PHASES* (Furey & Swaminathan, 1996). The phases used in these maps were calculated from the molecular-replacement solution. Two derivatives were identified in this way resulting from soaks in mercury chloride and platinum (IV) chloride. Native and derivative data were then scaled using *SCALEIT* (Collaborative Computational Project, Number 4, 1994) and phased with *MLPHARE* (Otwinowski, 1991). A difference Fourier map calculated using the anomalous data for the $HgCl_2$ derivative revealed peaks in the same positions as the isomorphous peaks and therefore these data were also included in the phasing calculation. When phased at 3.0 Å, these data produced an electron-density map that, whilst being the correct solution, was of insufficient quality to address the model errors, particularly in the critical loop regions (Fig. 1*b*). This was largely owing to the relatively poor quality of both derivatives, as judged by the merging statistics and completeness (Table 1). The resulting phases were improved spectacularly, however, by a combination of solvent flattening, histogram matching, twofold non-crystallographic symmetry (NCS) averaging and multi-crystal averaging as implemented in the program *DMMULTI* (Cowtan, 1994). The multi-crystal averaging component of this calculation was the inclusion of data from two different crystal forms of PGI. These were (i) the multiple isomorphous replacement (MIR) phases of the rabbit PGI structure to 3.0 Å resolution as described above and (ii) the MIR phases from pig muscle PGI, previously determined at 3.5 Å resolution using crystals of space group $P4_32_12$ (Shaw & Muirhead, 1977). The averaging domain used was a single monomer of PGI and the mask used was constructed from molecule *B* of the preliminary rabbit PGI coordinates. Since the rabbit PGI crystallizes as a dimer in the asymmetric unit, twofold non-crystallographic averaging was also performed. Solvent masks were calculated from the current models for rabbit and pig PGI. This phase-improvement procedure produced an excellent experimental density map that could be interpreted easily (Fig. 1*c*). A second equally interpretable electron-density map was calculated by solvent flattening

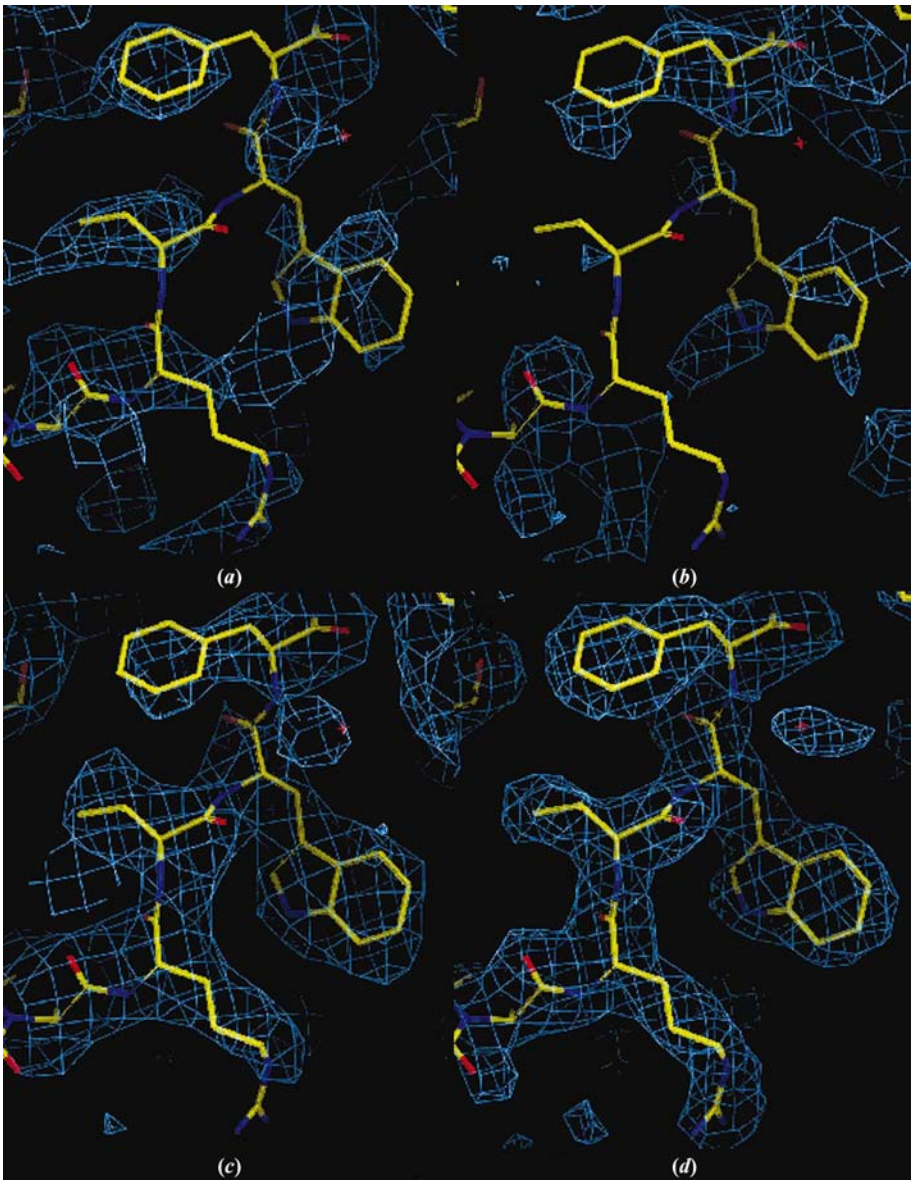

Figure 1
The improvement in the quality of the electron-density maps for rabbit PGI using non-crystallographic and multi-crystal averaging. The area shown is a typical loop region in which poor density had made model building difficult. These maps are displayed using the program *O* (Jones *et al.*, 1991) and are contoured at 1σ. (*a*) The phases obtained from a molecular-replacement solution using a preliminary structure of the pig enzyme as a search model. (*b*) MIR phases at 3.0 Å using derivative data from the $PtCl_4$ and $HgCl_2$ data sets. (*c*) The experimental density calculated at 3.0 Å using improved phases arising from NCS and multi-crystal averaging of the initial MIR phases. (*d*) The $2(|F_o| - |F_c|)$ density after the final refinement at 2.5 Å.

Table 2
Statistics of the final model.

Resolution range (Å)	15.0–2.5
σ cutoff applied	0.0
Total No. of reflections	42445
Percentage of reflections used in R_{free}	5.0
Completeness of data in resolution range (%)	93.9
No. of non-H protein atoms	8834
No. of water molecules	509
R factor (%)	18.1
R_{work} (%)	17.8
R_{free} (%)	23.4
R.m.s. deviations from ideal stereochemistry	
Bond lengths (Å)	0.010
Bond angles (°)	1.44
B factors	
Overall B factor	24.00
Mean B factor (main chain) (Å^3)	23.50
R.m.s. deviation in main-chain B factors (Å^3)	0.372
Mean B factor (side chains and waters) (Å^3)	24.45
R.m.s. deviation in side-chain B factors (Å^3)	1.23
Ramachandran plot	
Residues in most favoured region (%)	88.6
Residues in additionally allowed regions (%)	11.1
Residues in generously allowed regions (%)	0.0
Residues in disallowed regions (%)	0.2

and NCS averaging the MIR data using *DM* (Cowtan, 1994) and combining these phases with those obtained from the preliminary rabbit coordinates using *SIGMAA* (Read, 1986) (not shown).

2.4. Model building and refinement

The starting model for model building was the structure obtained by molecular replacement, *i.e.* a transformation of the preliminary pig structure. Using the program *O* (Jones *et al.*, 1991), the model was improved substantially and the sequence corresponding to rabbit PGI was inserted (Li & Chirgwin, 2000). Reference was made to both the multi-crystal averaged map and the phase-combined map. Refinements were carried out using *X-PLOR* (Brünger, 1992) and *REFMAC* (Murshudov *et al.*, 1997) alternating with further rounds of model building. In initial rounds the model was restrained to conform to NCS, but these restraints were later removed to allow the divergence of the two monomers in the dimer. In later stages water molecules were modeled and included in the refinement. Since in the native enzyme the N-terminal residue of PGI is an acetylated alanine (James & Noltmann, 1972), the final model is numbered 1–557. This model, which includes 509 water molecules, has an R factor of 18.1% and an R_{free} of 23.4% using all data to 2.5 Å and has excellent geometry (Table 2). The final electron density is shown in Fig. 1(*d*).

3. Results

3.1. Structure solution by multi-crystal averaging

After successful crystallization of rabbit PGI, a preliminary structure was obtained by molecular replacement using a partially refined pig structure as a search model, which was being determined in tandem with the rabbit enzyme. Phases calculated from this model, however, were of poor quality, necessitating the use of heavy-atom methods to solve the structure. After a search, two derivatives were obtained, but when used in phasing calculations the resulting MIR phases were of insufficient quality to improve the model. Ultimately, experimental phases of high quality were obtained using multi-crystal averaging using the MIR data of the rabbit enzyme and the 3.5 Å phases of PGI from pig enzyme (Shaw & Muirhead, 1977).

3.2. Structure description

The crystal structures of PGI reveal the enzyme to be a tight dimer of identical subunits (Fig. 2). The intimate association of the monomers is reinforced by an 'arm' at the C-terminus wrapping around the partner monomer, together with a similar feature on the opposite side of the molecule, termed the 'hook'. The two monomers forming the asymmetric unit of rabbit PGI can be superimposed with an r.m.s. deviation for all atoms of 0.88 Å (0.46 Å for C$^\alpha$ atoms) and can therefore be considered essentially identical. The structure consists of two domains, historically termed large and small (Shaw & Muirhead, 1977), although when compared with this 3.5 Å structure the two domains are now quite similar in size. This is a consequence, in part, of the addition of an extra β-strand and α-helix to the small domain. The structure of rabbit PGI has been described in detail elsewhere (Jeffery *et al.*, 2000). Briefly, the small domain comprises a five-stranded parallel β-sheet, packed on each side by three α-helices. The large domain is built around a six-stranded mixed parallel/antiparallel β-sheet packed on each side by four α-helices. The topology of this sheet is such that the outermost strands are formed first and the inner strands are formed last. Two interesting features of the structure are (i) a 48-residue extension at the C-terminus that extends away from the molecule and (ii) a 'hook' comprising two small α-helices (α20 and α21) that are connected to the molecule by a β-ribbon. Both of these features extend away from the monomer but make extensive contacts with the partner monomer in the dimer, so that the overall structure retains its globular characteristic. Ribbon representations of both the monomer and the dimer structure are shown in Fig. 2 together with the secondary-structure assignments.

3.3. Comparison with other PGIs

The crystal structures of PGI from three mammalian sources (pig, rabbit and human) are now known. In all cases the enzymes share essentially the same architecture, concordant with the high level of sequence identity seen within this group (85–95% identity). Most of the structures can be superimposed with an r.m.s. deviation in common main-chain atoms within the range 0.5–1.0 Å.

The overall fold of mammalian PGI is also similar to that of PGI from *B. stearothermophilus* (Sun *et al.*, 1999), but there are some significant differences consistent with the low level of sequence identity between mammalian and bacterial PGIs (typically 25%; Fig. 3). Taking monomer *A* of the rabbit

structure as an example, the common C^{α} atoms with the *Bacillus* enzyme superimpose with an r.m.s. deviation of 3.9 Å. Overall, the mammalian enzymes are larger owing to longer connections between secondary-structure elements, *e.g.* those between 106–119, 138–146 and 363–372, and including an extra 49 residues at the N-terminus. In the rabbit structure the latter comprises four α-helices (α1–α4) and β1 of the β-sheet in the large domain. Interestingly, the 30-residue connection between α19 and β6 (the hook) is absent in *Bacillus*, but instead a similar connection is located prior to this between β5 and α19 (mammalian nomenclature) (Fig. 3). This means that a stretch of residues (numbers 427–430, rabbit numbering) containing the highly conserved sequence Asn-Phe-Leu-Ala does not overlap structurally with its counterpart from *Bacillus*. A further difference is in the position of the C-terminal helix in *Bacillus*, which in the two structures is in different orientations. Despite the low level of sequence identity and the structural differences, the active-site architectures of the two enzymes are highly similar (see below).

3.4. Active-site region

Previous crystallographic studies of pig PGI located the active site of PGI to be in a cleft between the large and small domains, close to the dimer interface (Shaw & Muirhead, 1976). These studies also confirmed that there are two active

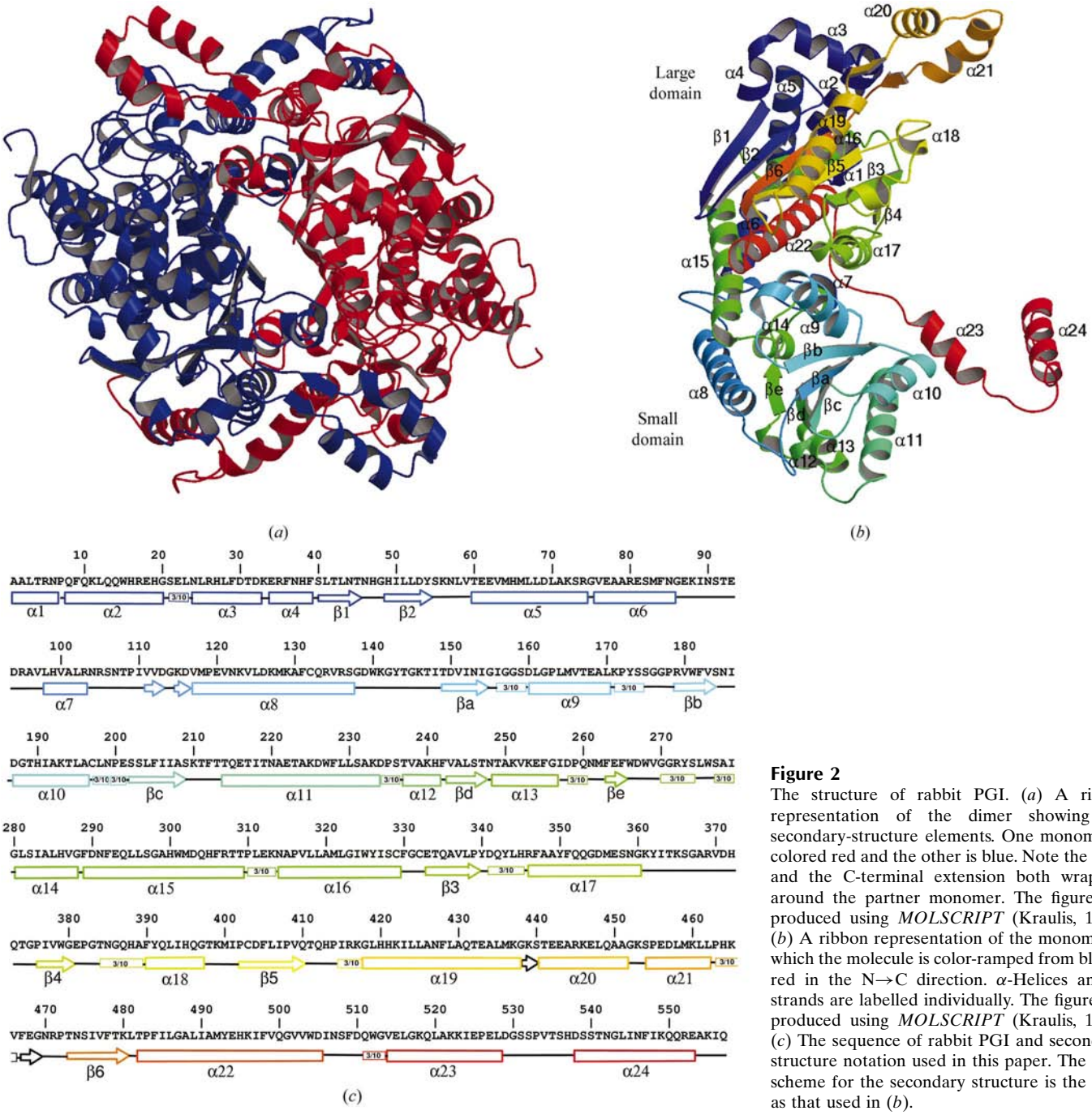

Figure 2
The structure of rabbit PGI. (*a*) A ribbon representation of the dimer showing the secondary-structure elements. One monomer is colored red and the other is blue. Note the hook and the C-terminal extension both wrapping around the partner monomer. The figure was produced using *MOLSCRIPT* (Kraulis, 1991). (*b*) A ribbon representation of the monomer in which the molecule is color-ramped from blue to red in the N→C direction. α-Helices and β-strands are labelled individually. The figure was produced using *MOLSCRIPT* (Kraulis, 1991). (*c*) The sequence of rabbit PGI and secondary-structure notation used in this paper. The color scheme for the secondary structure is the same as that used in (*b*).

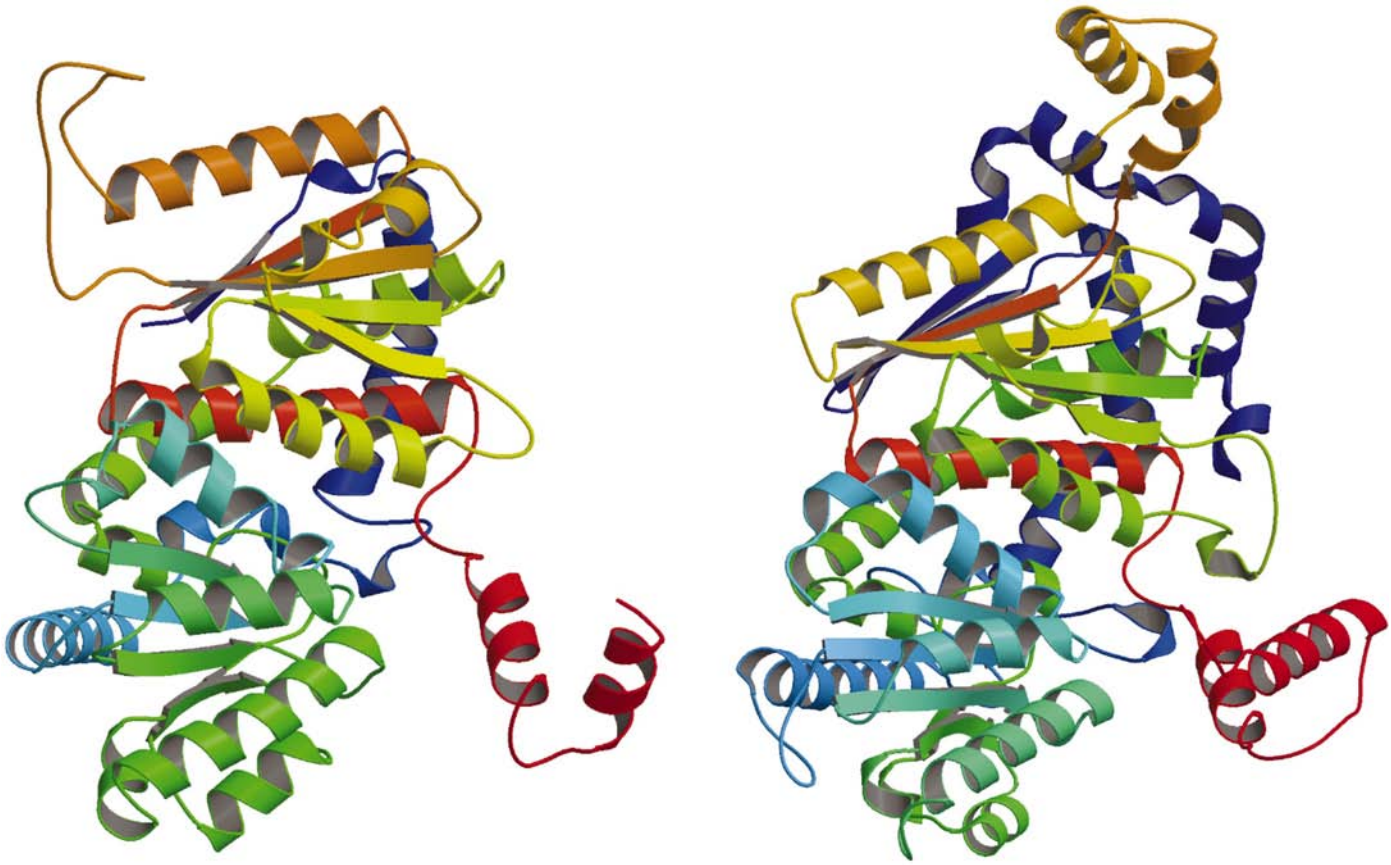

Figure 3
A structural comparison of phosphoglucose isomerase from *Bacillus* (left) and rabbit (right). The structure obtained from *B. stearothermophilus* (PDB code 2pgi) was superimposed onto the monomer *A* of the native rabbit structure and both folds are plotted in ribbon format. Each is colored blue to red, corresponding to the N-terminal to C-terminal direction. Note the additional series of α-helices at the N-terminus of the rabbit enzyme (colored in blue), which are all absent in the *Bacillus* enzyme. Note also the different locations of the 'hook' which, in this view, is located at the top right of the rabbit structure but is found at the top left of the *Bacillus* enzyme. This figure was prepared using *MOLSCRIPT* (Kraulis, 1991).

sites per dimer as had previously been deduced by inhibitor labeling (Bruch *et al.*, 1973). Recent crystal structures of the rabbit enzyme bound to inhibitor or substrate molecules in rabbit (Jeffery *et al.*, 2000, 2001; Lee *et al.*, 2001) and *Bacillus* (Chou *et al.*, 2000) have confirmed this location.

The active site of rabbit PGI is comprised of several different loops (Fig. 4). Many of these are the connections between the C-terminal ends of β-strands and the N-terminal ends of α-helices in the small domain, *i.e.* the connections βa–α9, βb–α10, βc–α11 and βe–α14. Other components include the C-terminal region of α17, the N-terminal region of α23 and the middle section of α19. An additional component, α18 and its preceding 3_{10}-helix, is contributed by the adjacent monomer in the dimer. Thus, each active site contains elements from both monomers and this is in accordance with biochemical data showing that dimers are required for activity (Bruch *et al.*, 1976).

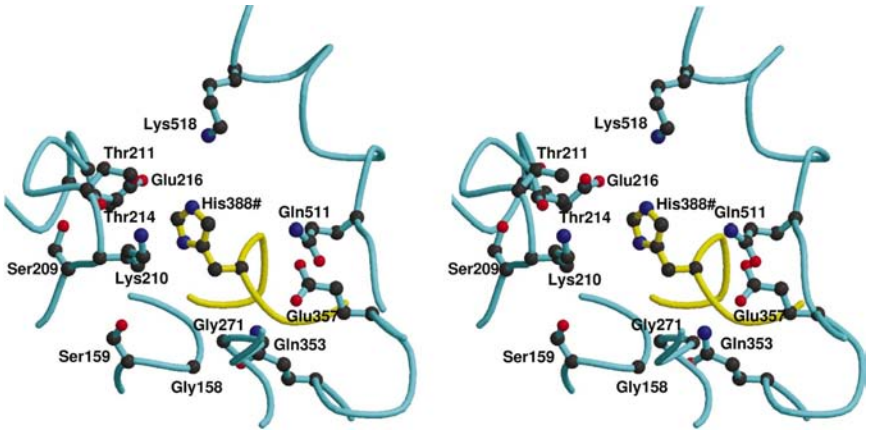

Figure 4
A stereoview of the active-site region of rabbit PGI showing important residues for substrate binding and catalysis, including the putative base catalyst Glu357. The main chain from monomer *A* is colored blue and that from monomer *B* is yellow. Note: # denotes residues from the adjacent monomer. The figure was produced using *MOLSCRIPT* (Kraulis, 1991).

The precise geometry of the active-site region is underpinned by numerous interactions between conserved residues. A few residues are particularly crucial and worthy of mention.

Arg272 links a 3_{10}-helix located between βe and α14 to helices α17 and α24 *via* interactions with the carbonyl O atoms of Ser508 and Asp510, Gln511 O^{ε} and the carboxylate group of Glu357. Arg272 could be the essential arginine identified by chemical labeling (Lu *et al.*, 1981). The same region is also stabilized by hydrogen bonds between Lys361 and the carbonyl O atoms of Asn509, Asp510, Ser358 and a likely electrostatic interaction with Asp510. Another important residue is Gln353, which forms a hydrogen bond *via* its O^{ε} to the carbonyl O atom of Gly159, thus linking α17 to the N-terminal end of α9. Other conserved interactions include those between Tyr273 and Ser358, Glu494 and Arg103, Asn187 and Gly385 and, lastly, Gln392 and Gly360.

In the rabbit structure the two active sites can be superimposed almost exactly: the only residue with a differing position is Lys518 which in molecule *B* has weak density, whereas in molecule *A* it is well resolved. The possible flexibility of this residue is consistent with its putative role in catalysis as discussed later. Both active sites contain several ordered water molecules, but few are spatially conserved between each active site in the dimer and many are presumably displaced upon substrate binding. All of the amino acids forming the active-site pocket are totally conserved. One of the most obvious features is a clustering of several serine and threonine residues to the left of the active site as viewed in Fig. 4. This includes threonines 211, 214 and 217 and serines 159 and 209. These residues are responsible for positioning the phosphate moiety of the substrate (Lee *et al.*, 2001) through a network of hydrogen-bonding interactions. There are also several glycine residues, 270, 271, 157 and 158, whose lack of side chain permits the close approach of the substrate molecule. Some of the remaining residues are likely candidates for having a role in catalysis, including Lys210, Glu357, Lys518 and His388# (where # denotes from the opposite monomer). Most of these residues appear to be free of contacts and available to interact with the substrate. His388 is notable because it forms a cross-subunit interaction with Glu216. Lys210 contacts the side chain of Asp267 and the carbonyl O atom of Phe265 *via* potential hydrogen bonds, but the density indicates that N^{ζ} may occupy two sites, indicating some flexibility in this side chain.

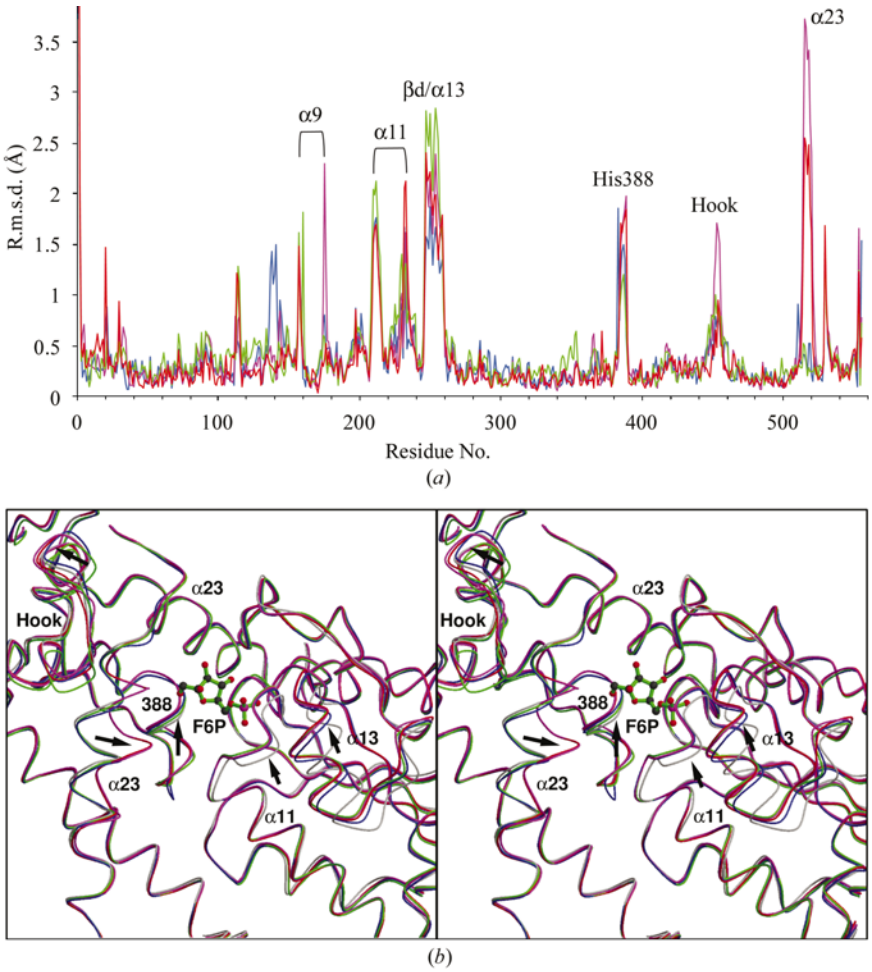

Figure 5
A comparison of native PGI with published structures of rabbit PGI complexed with 6-phosphogluconate (6PG), 5-phosphoarabinonate (PAB), 5-phosphoarabinonohydroxamic acid (PAH) and fructose 6-phosphate (F6P). (*a*) The r.m.s. deviations in main-chain atoms between native and the ligand-bound structures of rabbit PGI plotted per residue. The lines are colored blue for 6PG, purple for PAB, red for PAH and green for F6P. Areas showing significant changes between the native and ligand-bound enzymes are indicated. (*b*) A stereo representation of the superimposition of the backbone native and ligand-bound structures, showing the clustering of structural changes around the active site. The backbone of each structure is colored as in (*a*), but with the addition of the native structure in gray. Major structural features of the active site are labeled and regions of conformational change are indicated with arrows. The figure was produced using *MOLSCRIPT* (Kraulis, 1991).

3.5. Comparison with active site of PGI from *B. stearothermophilus*

Despite the structural differences between PGIs from mammalian and *B. stearothermophilus* sources noted earlier, the active sites in all species are highly similar, suggesting a common catalytic mechanism. Accordingly, PGI in *Bacillus* has active-site equivalents for Glu357 (Glu285), lysines 210 and 518 (Lys139 and Lys420), Arg272 (Arg202) and His388# (His306#). The intersubunit interaction between between Glu216 and His388# is also conserved in *Bacillus* as Glu145 and His306#. In addition, the same clustering of threonine and serines occurs in the phosphate-binding regions, together with a similar distribution of glycine residues.

3.6. Comparison with ligand-bound rabbit PGIs

Several structures of rabbit PGI complexed with inhibitors are known, but until now none of these has been compared with a rabbit native structure, preventing a

full description of any conformational changes associated with inhibitor binding. These are complexes with 6-phosphogluconate (6PG; Jeffery *et al.*, 2000), 5-phosphoarabinonate (PAB; Jeffery *et al.*, 2001) and 5-phosphoarabinonohydroxamic acid (PAH; Arsenieva *et al.*, 2002). The latter differs from PAB only very slightly; indeed, both structures are highly similar and can be treated as being essentially the same. A structure complexed with the closed form of the substrate fructose 6-phosphate (F6P) is also known (Lee *et al.*, 2001). The rabbit native structure superimposes very closely with all four of these structures, indicating that overall the global fold is retained upon ligand binding. The r.m.s. deviations between all main-chain atoms of the native enzyme and the respective ligand-bound structures are 0.62 Å for 6PG, 0.70 Å for PAB, 0.69 Å for PAH and 0.67 Å for F6P.

The r.m.s. deviations are shown plotted with residue number in Fig. 5(*a*). The largest structural differences between the native enzyme and the ligand-bound structures map to three regions of the molecule, all of which are clustered around the active site. The same changes are seen when comparing either monomer of the dimer. These are (i) a region of the small domain, (ii) the 3_{10}-helix preceding α18 and (iii) helix α23 (Fig. 5*b*). The hook structure also shifts slightly but will not be discussed further. These changes are significant because they involve residues that contact the substrate and may shed light onto the role of these in the reaction mechanism.

3.6.1. Small domain. The changes in the small domain map to two stretches of contiguous residues which are displaced in all four ligand-bound structures relative to the native enzyme (Fig. 6*a*). The largest shift occurs in residues 246–261, which comprises helix α13, its connecting loops and a stretch of 3_{10}-helix between residues 258 and 261. A second stretch of chain between residues 209 and 241 also shifts but with a smaller magnitude. This comprises α11, α12 and their

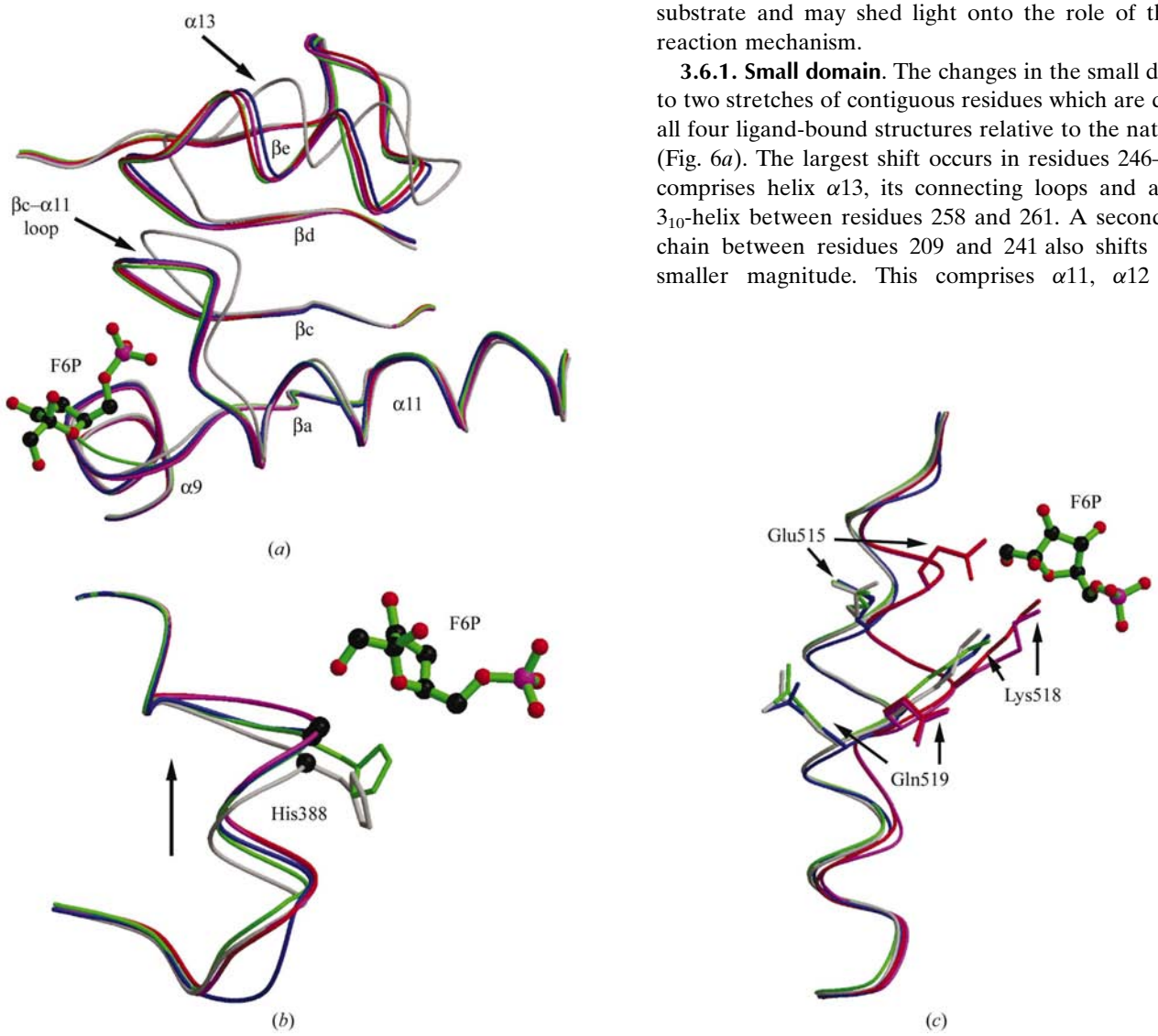

Figure 6
Details of the three regions showing significant structural changes between native and ligand-bound forms of rabbit PGI. In all cases the color scheme is the same as in Fig. 4. For reference, a ball-and-stick representation of the substrate fructose 6-phosphate is shown with its bonds colored green, the same as its backbone. All figures were produced using *MOLSCRIPT* (Kraulis, 1991). (*a*) A close-up of the small domain showing the shifts of α13 and of the loop between βc and α11 that closes around the phosphate group of the sugar substrate. (*b*) The shift in the 3_{10}-helix bearing His388 toward the substrate. The side chain of His388 is shown in the native structure with gray bonds and in the F6P-bound structure with green bonds. Note both the shift and the rotation in this residue. (*c*) The movement of helix α23 upon binding 5-phosphoarabinonate (PAB) and 5-phosphoarabinonohydroxamic acid (PAH). Note how in this region the 6PG and F6P-bound structures overlap closely with the native structure. Residues within α23 that shift significantly are shown as bonds using the same colors as their respective backbones and the two positions are indicated by arrows. Note also the almost exact superimposition of the PAB- and PAH-bound structures.

connecting loops. The largest shift is observed in the F6P-bound structure, whereas the shifts in the 6PG, PAB and PAH structures are similar in magnitude.

This part of the PGI structure forms the binding site for the phosphate group of the substrate molecules by providing a constellation of threonine and serine residues that interact with the phosphate O atoms either directly or *via* bridging water molecules (Jeffery *et al.*, 2000; Read *et al.*, 2001). The effect of the structural changes is to bring these residues closer to the phosphate group so as to lock around the substrate molecule upon binding.

3.6.2. 388 region. Residues 383–389, which form a 3_{10}-helix, shift toward the active site in all four ligand-bound structures (Fig. 6*b*). The greatest movement is seen in the PAB/PAH structures, with lesser movement in the F6P and 6PG structures. The most prominent residue of this helix is His388. Its C^{α} atom moves 1.7 Å in the PAB/PAH structures and around 1.2 Å in the 6PG and F6P structures. In addition, in all the ligand-bound structures the side chain of His388 is rotated around the $C\alpha-C\beta$ bond such that N^{δ} of the imidazole ring is brought to within hydrogen-bonding range to O5 (the ring oxygen) of F6P or its equivalent (O4) in the inhibitor molecules.

3.6.3. Helix *α*23. In contrast to the changes in the small domain, which occur in all four ligand-bound structures, the shift of helix α23 toward the substrate-binding site is seen only in the PAB/PAH structures (Fig. 6*c*). Interestingly, this is the only region in which the PAB-bound and PAH-bound enzymes differ. In the PAH-bound structure, α23 moves in a similar manner to the PAB-bound structure, but this accompanied by a slight unwinding of the helix so that it now tends toward a 3_{10}-helix in its conformation.

The structural differences between the native enzyme and the PAB/PAH structures include residues 512–522, which is the N-terminal half of the helix. The most significant changes occur in residues 514, 515 and 518. In the PAB/PAH structures Val514 has moved toward the C1 and C2 position of the inhibitors, which are equivalent to C3 and C4 of the open-chain substrate. Since the C1 and C2 O atoms are projecting away, this region of the inhibitor presents a hydrophobic face to the valine. Glu515 is interesting because not only has this residue moved as a whole, but also its side chain has bent around to point toward the active site. In so doing, a salt bridge between Glu515 and Lys465 in the native enzyme is broken and in the PAB/PAH structures this residue now makes water-mediated contacts with both O1 of the inhibitor and Lys518 N^{ζ}. Another important consequence of the shift in α23 is the relative movement of Lys518. Comparing wild-type and PAB-bound enzymes, C^{α} of this residue shifts 3 Å and its N^{ζ} atom shifts by 5.5 Å. This movement brings N^{ζ} into direct contact with PAB (and PAH), so that in the PAB structure it is 3.0 Å from O4 and 3.1 Å from O5 of the inhibitor. A further difference of note concerns Gln519, which in the native enzyme hydrogen bonds to Lys439 and Glu447 of the opposite monomer; in the PAB/PAH structures these contacts are broken. The possible roles of Glu515 and Lys518 in the mechanism of PGI are discussed below.

4. Discussion

4.1. Structure determination

The process leading to the current structure for rabbit PGI has been a complicated one. The earlier previous crystallographic studies were of the enzyme from pig muscle (Shaw & Muirhead, 1977; Achari *et al.*, 1981), but these stalled owing to the lack of high-quality phases that were needed to correct the many errors in the model (Davies & Muirhead, unpublished work). PGI from rabbit muscle is commercially available and is a convenient source of the enzyme. It was therefore decided that a whole new determination should be carried out with this enzyme. Following its successful crystallization, the rabbit structure could be positioned using molecular replacement with the best available pig structure as a search model. At that time, however, the pig structure was only partially refined, hence the quality of the resulting phases from molecular replacement was poor, precluding any meaningful corrections to the rabbit structure. Thus, it was decided that obtaining unbiased experimental phases would be the best means of solving the problem. A derivative search yielded two candidates. One of these [platinum (IV) chloride] had a relatively weak signal through low occupancy and the other data set [mercury (II) chloride] was marred by its lack of completeness. An MIR map calculated from these data was interpretable in parts, but the critical loop regions were not well resolved (Fig. 1*b*).

The key to solving the structure was to combine information from two species of PGI and hence two different crystal forms of PGI, including the rabbit MIR phases and the 3.5 Å phases from the original structure determination of the enzyme from pig muscle (Shaw & Muirhead, 1977). The resulting improvement in phases was substantial (see Fig. 1) and finally a model could be built based on accurate experimental phase information. In turn, the refined rabbit structure was used to correct the errors in the pig structure (Davies & Muirhead, 2002).

4.2. Dimer structure

The available structures of PGI show that the molecule is a tight dimer of identical subunits, consistent with biochemical evidence that a dimer is necessary for enzyme activity (Bruch *et al.*, 1976). The dimer appears to be held together in part by intermolecular interactions between the 'hook' and, more importantly, the C-terminal part of the molecule, both of which wrap around the accompanying monomer. The long extension at the C-terminal end of the protein appears to be a further example of 'domain swapping', where monomers become dimers by exchanging sections of their structure (for a review, see Ostermeier & Benkovic, 2000). In the case of PGI this appears to have been a crucial step in the evolution of the enzyme, since the active site is comprised of chains from both monomers and, importantly, residues from the C-terminal region contribute to the active site.

4.3. Reaction mechanism

There are two components of the catalytic reaction of PGI: the transfer of the carbon-bound hydrogen between C1 and C2 and the prerequisite step of ring opening (see Fig. 7). The hydrogen transfer could occur by one of two mechanisms: as a proton *via* a *cis*-enediolate intermediate or as a direct hydride transfer (Rose, 1975). Since most studies detect at least some degree of hydrogen exchange with solvent (*e.g.* Rose & O'Connell, 1961), the reaction is considered to be a proton transfer with a *cis*-enediolate intermediate. This mechanism is common in many aldose–ketose isomerases, including the best characterized enzyme, triose phosphate isomerase (TIM). By contrast, xylose isomerase, which contains divalent cations at the active site, does not show hydrogen exchange with the solvent and is proposed to instead operate *via* a direct hydride shift (Collyer & Blow, 1990; Farber *et al.*, 1989; Whitlow *et al.*, 1991). The same may also be true for other aldose–ketose isomerases containing divalent cations at their active sites, *e.g.* rhamnose isomerase (Korndorfer *et al.*, 2000). For the ring-opening step, the enzyme is likely to contain an acid catalyst that protonates the ring oxygen to a hydroxyl group.

4.3.1. Base catalyst for isomerase activity. In the general acid–base mechanism proposed for PGI, the enzyme provides a base for proton abstraction at the C2 position of G6P and C1 position of F6P. When relating the structures of PGI to its isomerase mechanism, two such candidates for base catalyst have been proposed: His388 and Glu357. Based on crystal structures of rabbit PGI bound to 6PG (Jeffery *et al.*, 2000) and of *Bacillus* PGI bound to PAB (Chou *et al.*, 2000), initial interest centred on His388 (His306 in *Bacillus*). In these structures, His388 was interpreted as being close enough to abstract a protein from C1/C2 of the substrates. In addition, in all known structures of PGI, His388 interacts with Glu216 across the subunit boundary (His308 and Glu145, respectively, in *Bacillus*), an arrangement which is reminiscent of the His-Asp charge couple in serine proteases. This interaction was postulated to increase the basicity of the histidine for proton abstraction (Chou *et al.*, 2000; Jeffery *et al.*, 2000) and, indeed, mutation of the equivalent histidine in *B. stearothermophilus* (His308) to alanine, asparagine or glutamine lowered k_{cat} by a factor of 10^3 (Meng *et al.*, 1999). A role for histidine in the catalytic mechanism of PGI is also supported by chemical labeling experiments (Gibson *et al.*, 1980) and by kinetic data, which showed an ionizable group with pK_a values in the range 6.0–6.9 (Dyson & Noltmann, 1968; Hines & Wolf, 1963). However, in the 6PG rabbit structure (Jeffery *et al.*, 2000), His388 is too far away to contact either C1 or C2 of the inhibitor directly, requiring either a different binding mode for the true substrate or a movement of His388 when bound to substrate. Moreover, in the *Bacillus* PAB structure, the inhibitor has been modelled in an opposite orientation to that seen in structures of rabbit and pig PGI bound to the same inhibitor (Davies & Muirhead, 2002; Jeffery *et al.*, 2001), leading to a different conclusion regarding His306. Given the high specificity of PGI for phosphorylated sugars (see Noltmann, 1972), together with the precise nature of the inter-

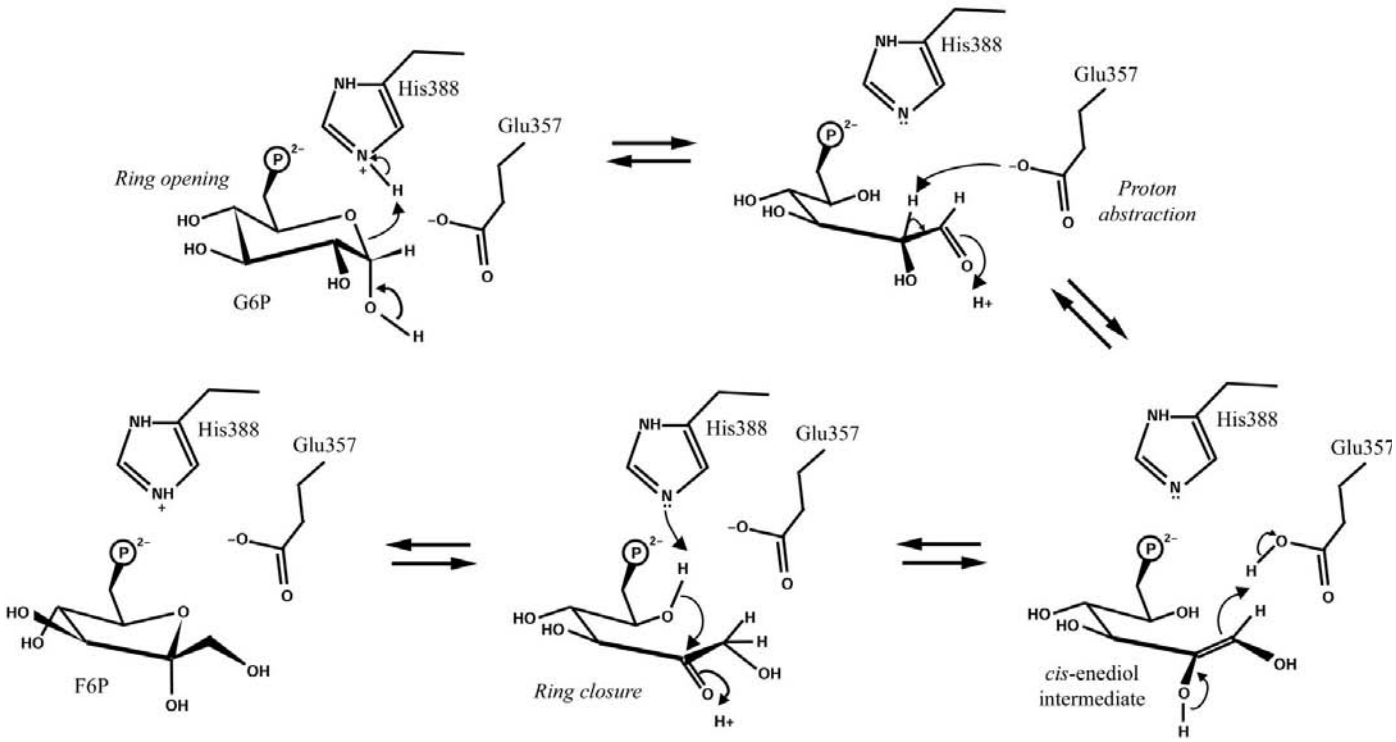

Figure 7
A catalytic mechanism for phosphoglucose isomerase, shown here in the glucose 6-phosphate to fructose 6-phosphate direction. The reaction comprises three steps: (i) ring opening, which is shown here to be acid catalysed by His388, (ii) isomerization *via* a *cis*-enediol intermediate, in which Glu357 transfers a proton from C2 of G6P to C1 of F6P, and (iii) ring closure, in which His388 promotes ring closure by abstracting a proton from the hydroxyl group on C5.

actions between the enzyme and phosphate seen in the structures of mammalian PGIs (Davies & Muirhead, 2002; Jeffery *et al.*, 2001), a different binding mode for PAB in *Bacillus* PGI seems improbable.

Recent crystal structures of human PGI (Read *et al.*, 2001) and of rabbit PGI bound to F6P (Lee *et al.*, 2001) and PAB (Jeffery *et al.*, 2001) have led to suggestions that a better candidate for base catalyst is Glu357 (Fig. 7). As best illustrated by the F6P-bound structure, this residue is well placed to abstract a proton directly from C1. By contrast, His388 is less well placed with respect to C1/C2 and instead makes contacts with the ring oxygen of the fructose substrate. An active-site glutamate has also been suggested by chemical labeling with 1,2-anhydro-D-mannitol 6-phosphate (O'Connell & Rose, 1973). Moreover, the bidentate character of this residue would facilitate abstraction and donation of the proton through either O^{ε} of the glutamate and such an arrangement may explain the relatively low level of hydrogen exchange with solvent (Rose & O'Connell, 1961). For Glu357 to act as base, however, would require an upward perturbation in its pK_a to reach the measured pK_a range of 6–7 and it remains unclear how this is achieved within the environment of the active site.

A glutamate base catalyst in the active site of PGI raises the prospect that the isomerase mechanism for PGI may in fact be very similar to that of triose phosphate isomerase. TIM uses a glutamate (Glu165) as a catalytic base for proton abstraction and a positively charged group, His95, for stabilizing the enediolate ion (Raines *et al.*, 1986). The equivalent residue to His95 may be Arg272, which is immediately adjacent to Glu357 and may counteract the transient negative charge of the enediolate intermediate (Lee *et al.*, 2001).

4.3.2. Ring opening. Several lines of evidence suggest that PGI catalyses opening of the sugar ring prior to the isomerase reaction. Firstly, the open-chain forms of glucose and fructose are present in only trace amounts in solution (Swenson & Barker, 1971) and it is assumed that proportions are also found of the phosphorylated forms of the sugars. Secondly, the high catalytic efficiency of PGI is inconsistent with the enzyme utilizing the less abundant open-chain forms of the sugar substrates. Finally, PGI can catalyse the anomerization, but not the isomerization, of mannose 6-phosphate (Rose *et al.*, 1973), indicating that this activity is functionally and perhaps spatially separate from the isomerase reaction. A further question regarding the mechanism of PGI therefore pertains to the group responsible for ring opening. Based on the available crystal structures of PGI, there are two likely candidates: His388 and Lys518.

In all four ligand-bound structures of rabbit PGI, the δ ring nitrogen of His388 lies in the range 2.6–2.9 Å away from O5 of the substrate or its equivalent in the inhibitor molecules. In this position, His388 could act as the acid group that catalyses ring opening by donating a proton to the ring oxygen (Fig. 7). In this case, His388 would exist in the imidazolium form prior to catalysis. The other possibility is that Lys518 acid catalyses ring opening. In the F6P-bound structure Lys518 N^{ζ} is distant from O5, but in the PAB structure it has moved to within 3 Å of the equivalent atom (O4). The participation of a lysine residue in the catalytic mechanism of PGI has been suggested by kinetic studies, which reveal an ionizable group with an apparent pK_a in the range 9–10 (Dyson & Noltmann, 1968; Hines & Wolf, 1963; Marchand *et al.*, 1989) and by chemical labeling with pyridoxal 5-phosphate (Lu *et al.*, 1981; Palmieri *et al.*, 1982). The large shift in α23 seen in the PAB/PAH structures is further evidence that Lys518 plays a significant role in the catalytic mechanism. If it plays no direct part in ring opening, then Lys518 is likely to have another role such as transferring a proton between the C1 and C2 hydroxyl positions *via* interactions with active-site waters, as has been suggested by Lee *et al.* (2001).

4.4. Conformational changes associated with catalysis

The putative roles of particular residues in the reaction mechanism can be examined in the light of conformational changes associated with catalysis that have been revealed by our comparison of native rabbit PGI with several structures of the same enzyme in complex with several inhibitors as well as with fructose 6-phosphate. The largest structural differences occur in three regions of the active site: in the small domain, in the 3_{10}-helix containing His388 and in helix α23 near the C-terminus. Interestingly, the helix carrying the putative base Glu357 (α27) does not appear to move upon binding ligand.

In the native enzyme, α13, the loop between βc and α11, and α11 are seen in an 'open' conformation, in which these elements lie further away from the active site than in the ligand-bound structures of the enzyme, which exhibit a 'closed' conformation. Since the 'closed' conformation is also observed in the structure of human PGI in which a sulfate moiety from the crystallization solution occupies the phosphate position (Read *et al.*, 2001), it can be argued that recognition of the phosphate group of the substrate alone is the trigger for these structural movements. Accordingly, the magnitude of the structural change is similar in all four ligand-bound structures, even though the ligands differ in their structure beyond the phosphate group, *e.g.* open-chain *versus* closed chain. The purpose of this movement is to close the constellation of serine and threonine groups, as well the amide N atoms of residues 210 and 211, onto the phosphate group of the substrate. The precision of this interaction explains why PGI has such a high specificity for phosphorylated sugars (Noltmann, 1972).

The second major structural difference between the native enzyme and available ligand-bound structures is the movement of helix α23. Such a shift was first noted in a preliminary structure of pig PGI complexed with PAB resolved at 3.5 Å (Shaw & Muirhead, 1976). This structure has since been refined and shows an almost identical shift in α23 as seen here in the rabbit enzyme (Davies & Muirhead, 2002). Interestingly, this helix is displaced toward the active site only in the PAB and PAH structures and not in the F6P or 6PG structures. Since PAB (and PAH) closely mimics the presumed transition-state analogue, this structure is likely to represent a snapshot of a conformational state that occurs during catalysis. The

main consequence of this shift is to bring Lys518 into contact with both O4 and O5 of the PAB/PAH inhibitors, which represents a movement of over 5 Å for N^{ζ}. As discussed above, this makes Lys518 a candidate for having a role in ring opening. Another striking change occurs in Glu515, whose side chain moves such that a salt bridge to Lys465 in the native structure is broken and the residue forms new contacts with both the PAB/PAH inhibitor and Lys518 *via* water molecules. The displacement of both O^{ε} atoms is over 7 Å. The end result is that Glu515 forms a link between Lys518 and the O1 position of PAB through interactions with water molecules. It also makes a direct contact with Gln511. The proximity of the glutamate to Lys518 may influence the pK_a of the lysine to promote ring opening or, equally, it may help facilitate the movement of the hydroxyl protons in the isomerase reaction.

The third movement shifts a 3_{10}-helix bearing His388 toward the substrate to bring this residue into close proximity with the ring oxygen. In the native structure, His388 contacts Glu216 of the adjacent monomer in an interaction which may serve to tether elements of the active site that emanate from different monomers. An alternative explanation is that this interaction alters the pK_a of His388 to promote its function in ring opening. A notable strengthening of this interaction in all four ligand-bound forms of the rabbit enzyme supports the latter hypothesis. In the native structure OE1 and OE2 of Glu216 are 4 and 3.4 Å, respectively, from N^{ε} of the imidazole ring, whereas in the PAB structure the respective distances are now 3.2 and 3.3 Å.

4.4.1. Sequence of conformational changes. The temporal sequence of the three identified conformational changes during the catalytic cycle can only be surmised, but a likely scenario is as follows. The initial event in substrate binding is the recognition of the phosphate group, which then induces the first conformational change in the small domain, resulting in α13 shifting toward the phosphate. The next structural shifts could be the 3_{10}-helix carrying His388 or helix α23, moving either in tandem or sequentially. However, since the inward movement of α23 is blocked in the F6P-bound structure by a steric clash between the C1 region of the substrate and Val514 (Lee *et al.*, 2001) and since also in this structure the 3_{10}-helix is partially displaced toward the active site, the movement of His388 toward the ring oxygen is likely to occur first. This suggests that α23 can only move after the steric clash with Val514 has been relieved by ring opening and therefore supports the hypothesis that His388 is responsible for ring opening and not Lys518, which at that stage is too far away to interact with O5 (Fig. 7). The role this leaves for Lys518 is to facilitate transfer of the oxygen-bound proton between the C1 and C2 O atoms. After isomerization the same steps occur in reverse, beginning with the retreat of α23, followed by ring closure and the shift in His388; after the product is released, α13 and accompanying structural elements in the small domain relax to the open conformation. Any one of these movements could be the prerequisite conformational change that is the rate-limiting step in the catalytic activity of yeast PGI (Malaisse *et al.*, 1990).

Assessing the veracity of this scheme will require further structures. One key issue to be resolved is whether the shift in helix α23 does indeed occur with the true substrates. Whilst the structure of PAB (and PAH) is presumed to resemble the transition-state analogue, the position of α23 seen in the enzyme bound to this inhibitor could instead represent the enzyme in an anomalous and inactivated conformation. The available structure of PGI bound to F6P shows the fructose is observed in ring form and is likely to represent the enzyme state immediately prior to product release, but a snapshot of the enzyme prior to this state in which the substrate is in open-chain form is also required.

5. Conclusion

In this paper, we have used the native structure of rabbit PGI to describe three conformational changes in the structure that are associated with its catalytic function and we have also presented a model of the temporal sequence of these changes. By correlating these structural movements with the likely functions of individual amino acids in the active site, we have also provided further insight into the catalytic mechanism. Glu357 remains the best candidate as base catalyst, but these studies also add weight to the hypothesis that His388 participates in the ring-opening process. On a cautionary note, however, the uncertainty of assigning specific functions to residues is amply illustrated by His388. To date, a single group has ascribed three different functions to this residue: namely, base catalyst in the isomerase reaction (Jeffery *et al.*, 2000), as a proton acceptor in ring opening (Jeffery *et al.*, 2001) and, most recently, as the acid catalyst for ring opening (Lee *et al.*, 2001). Clearly, further elucidation of the precise roles individual amino acids play in the catalytic function of PGI will require mutational and kinetic data in combination with additional structural studies.

The authors acknowledge the support of the American Lebanese Syrian Associated Charities (ALSAC) for the X-ray facilties at St Jude Children's Research Hospital, Memphis, TN, USA. We are also grateful to John Chirgwin for providing the sequence of rabbit PGI in advance of publication. HM is supported by an Emeritus Fellowship from the Leverhulme Trust.

References

Achari, A., Marshall, S. E., Muirhead, H., Palmieri, R. H. & Noltmann, E. A. (1981). *Philos. Trans. R. Soc. London Ser. B*, **293**, 145–157.

Arsenieva, D., Hardre, R., Salmon, L. & Jeffery, C. J. (2002). *Proc. Natl Acad. Sci. USA*, **99**, 5872–5877.

Baughan, M. A., Valentine, W. N., Paglia, D. E., Ways, P. O., Simons, E. R. & Demarsh, Q. B. (1968). *Blood*, **32**, 326–249.

Baumann, M., Kappl, A., Lang, T., Brand, K., Siegfried, W. & Paterok, E. (1990). *Cancer Invest.* **8**, 351–356.

Bruch, P., Schnackerz, K. D., Chirgwin, J. M. & Noltmann, E. A. (1973). *Eur. J. Biochem.* **36**, 564–568.

Bruch, P., Schnackerz, K. D. & Gracy, R. W. (1976). *Eur. J. Biochem.* **68**, 153–158.

Brünger, A. T. (1992). *X-PLOR Version 3.1. A System for X-ray Crystallography and NMR.* Yale University, New Haven, CT, USA.
Cao, M. J., Osatomi, K., Matsude, R., Ohkubo, M., Hara, K. & Ishihara, T. (2000). *Biochem. Biophys. Res. Commun.* **272**, 485–489.
Chaput, M., Claes, V., Portetelle, D., Cludts, I., Cravador, A., Burny, A., Gras, H. & Tartar, A. (1988). *Nature (London)*, **332**, 454–455.
Chou, C.-C., Sun, Y.-J., Meng, M. & Hsiao, C.-D. (2000). *J. Biol. Chem.* **275**, 23154–23160.
Collaborative Computational Project, Number 4 (1994). *Acta Cryst.* D**50**, 760–763.
Collyer, C. A. & Blow, D. M. (1990). *Proc. Natl Acad. Sci. USA*, **87**, 1362–1366.
Cowtan, K. (1994). *Jnt CCP4/ESF–EACBM Newsl. Protein Crystallogr.* **31**, 34–38.
Davies, C. & Muirhead, H. (2002). *Proteins Struct. Funct. Genet.* **49**, 577–579.
Dyson, J. E. D. & Noltmann, E. A. (1968). *J. Biol. Chem.* **243**, 1401–1414.
Faik, P., Walker, J. I., Redmill, A. A. & Morgan, M. J. (1988). *Nature (London)*, **332**, 455–457.
Farber, G. K., Glasfield, A., Tiraby, G., Ringe, D. & Petsko, G. A. (1989). *Biochemistry*, **28**, 7289–7297.
Furey, W. & Swaminathan, S. (1996). *Methods Enzymol.* **277**, 590–620.
Gibson, D. R., Gracy, R. W. & Hartmann, F. C. (1980). *J. Biol. Chem.* **255**, 9369–9374.
Gurney, M. E. (1988). *Nature (London)*, **332**, 458.
Gurney, M. E., Apatoff, B. R., Spear, G. T., Baumel, M. J., Antel, J. P., Bania, M. B. & Reder, A. T. (1986). *Science*, **234**, 574–581.
Gurney, M. E., Heinrich, S. P., Lee, M. R. & Yin, H. S. (1986). *Science*, **234**, 566–573.
Hines, H. C. & Wolf, R. G. (1963). *Biochemistry*, **2**, 770–775.
James, G. T. & Noltmann, E. A. (1972). *J. Biol. Chem.* **248**, 730–737.
Jeffery, C. J., Bahnson, B. J., Chien, W., Ringe, D. & Petsko, G. A. (2000). *Biochemistry*, **39**, 955–964.
Jeffery, C. J., Hardre, R. & Salmon, L. (2001). *Biochemistry*, **40**, 1560–1566.
Jones, T. A., Zou, J.-Y., Cowan, S. W. & Kjeldgaard, M. (1991). *Acta Cryst.* A**47**, 110–119.
Korndorfer, I. P., Fessner, W. D. & Matthews, B. W. (2000). *J. Mol. Biol.* **300**, 917–933.
Kraulis, P. J. (1991). *J. Appl. Cryst.* **24**, 946–950.
Lee, J. H., Chang, K. Z., Patel, V. & Jeffery, C. J. (2001). *Biochemistry*, **40**, 7799–7805.
Li, X. & Chirgwin, J. M. (2000). *Biochim. Biophys. Acta*, **1476**, 363–367.
Lu, H. S., Talent, J. M. & Gracy, R. W. (1981). *J. Biol. Chem.* **256**, 785–793.
Malaisse, W. J., Malaisse-Lagae, F., Liemans, V., Ottinger, R. & Willem, R. (1990). *Mol. Cell. Biochem.* **93**, 153–165.
Marchand, M., Kooysra, U., Wierenga, R. K., Lambier, A. M., van Beeuman, J., Opperdoes, F. R. & Michels, P. A. M. (1989). *Eur. J. Biochem.* **184**, 455–464.
Matsumoto, I., Staub, A., Benoist, C. & Mathis, D. (1999). *Science*, **286**, 1732–1735.
Meng, M., Chane, T. L., Sun, Y. J. & Hsiao, C. D. (1999). *Protein Sci.* **8**, 2438–2443.
Murshudov, G. N., Vagin, A. A. & Dodson, E. J. (1997). *Acta Cryst.* D**53**, 240–255.
Navaza, J. (1994). *Acta Cryst.* A**50**, 157–163.
Noltmann, E. A. (1972). *The Enzymes*, edited by P. D. Boyer, pp. 271–354. New York: Academic Press.
O'Connell, E. L. & Rose, I. A. (1973). *J. Biol. Chem.* **248**, 2225–2231.
Ostermeier, M. & Benkovic, S. J. (2000). *Adv. Protein Chem.* **55**, 29–77.
Otwinowski, Z. (1991). *Proceedings of the CCP4 Study Weekend. Isomorphous Replacement and Anomalous Scattering*, edited by W. Wolf, P. R. Evans & A. G. W. Leslie, pp. 80–88. Warrington: Daresbury Laboratory.
Otwinowski, Z. & Minor, W. (1997). *Methods Enzymol.* **276**, 307–326.
Palmieri, R. H., Gee, D. M. & Noltmann, E. A. (1982). *J. Biol. Chem.* **257**, 7965–7968.
Raines, R. T., Sutton, E. L., Straus, D. R., Gilbert, W. & Knowles, J. R. (1986). *Biochemistry*, **25**, 7142–7154.
Read, J., Pearce, J., Li, X., Muirhead, H., Chirgwin, J. & Davies, C. (2001). *J. Mol. Biol.* **309**, 447–464.
Read, R. J. (1986). *Acta Cryst.* A**42**, 140–149.
Rose, I. A. (1975). *Adv. Enzymol. Relat. Areas Mol. Biol.* **43**, 491–517.
Rose, I. A. & O'Connell, E. L. (1961). *J. Biol. Chem.* **236**, 3086–3092.
Rose, I. A., O'Connell, E. L. & Schray, K. J. (1973). *J. Biol. Chem.* **248**, 2232–2234.
Shaw, P. J. & Muirhead, H. (1976). *FEBS. Lett.* **65**, 50–55.
Shaw, P. J. & Muirhead, H. (1977). *J. Mol. Biol.* **109**, 475–485.
Sun, Y. J., Chou, C. C., Chen, W. S., Wu, R. T., Meng, M. & Hsiao, C. D. (1999). *Proc. Natl Acad. Sci. USA*, **96**, 5412–5417.
Swenson, C. A. & Barker, R. (1971). *Biochemistry*, **10**, 3151–3154.
Watanabe, H., Takehana, K., Date, M., Shinozaki, T. & Raz, A. (1996). *Cancer Res.* **56**, 2960–2963.
Whitlow, M., Howard, A. J., Finzel, B. C., Poulos, T. L., Winbourne, E. & Gilliland, G. L. (1991). *Proteins Struct. Funct. Genet.*, **9**, 153–173.
Xu, W., Seiter, K., Feldman, E., Ahmed, T. & Chiao, J. W. (1996). *Blood*, **87**, 4502–4506.
Yakirevich, E. & Naot, Y. (2000). *Biol. Reprod.* **62**, 1016–1023.